Soft Matter

Cite this: *Soft Matter*, 2012, **8**, 4687

www.rsc.org/softmatter

PAPER

Co-existence of gel and fluid lipid domains in single-component phospholipid membranes

C. L. Armstrong,*[a] M. A. Barrett,[a] L. Toppozini,[a] N. Kučerka,[b] Z. Yamani,[b] J. Katsaras,[bc] G. Fragneto[d] and M. C. Rheinstädter*[ab]

Received 11th November 2011, Accepted 21st February 2012
DOI: 10.1039/c2sm07158d

Lateral nanostructures in membranes, so-called rafts, are believed to strongly influence membrane properties and functions. The experimental observation of rafts has proven difficult as they are thought to be dynamic structures that likely fluctuate on nano- to microsecond time scales. Using neutron diffraction we present direct experimental evidence for the co-existence of gel and fluid lipid domains in a single-component phospholipid membrane made of DPPC as it undergoes its main phase transition. The coherence length of the neutron beam sets a lower limit for the size of structures that can be observed. Neutron coherence lengths between 30 and 242 Å used in this study were obtained by varying the incident neutron energy and the resolution of the neutron spectrometer. We observe Bragg peaks corresponding to co-existing nanometer sized structures, both in out-of-plane and in-plane scans, by tuning the neutron coherence length. During the main phase transition, instead of a continuous transition that shows a pseudo-critical behavior, we observe the co-existence of gel and fluid domains.

1 Introduction

Clusters, rafts, nanodomains, and patches have become a central issue in cell membrane studies.[1–4] The heterogeneous organization of membrane constituents is not only believed to be essential for cellular functions such as signalling, trafficking and adhesion,[5–7] but also impacts material properties.[8] However, the experimental observation of these heterogeneities has proven to be challenging, as they are thought to be short-lived.[9–12] As such, in order for experimental techniques to unambiguously observe such structures, they must be capable of simultaneously accessing small length scales and fast (nano to microsecond) time regimes.

Lipid bilayers are established model systems for studying dynamics and functional aspects of complex biological membranes.[13,14] They also allow the investigation of heterogeneous structures, which mimic "rafts". Submicron sized domains in ternary mixtures of phospholipids and cholesterol have been observed using small angle neutron scattering (SANS).[15–19] Selective deuteration was used in these experiments to enhance the scattering of the heterogeneities, and domains in the range 20–200 nm radius were observed. Domains in these so-called raft forming lipid mixtures are thermodynamically stable and quasi-static, *i.e.*, changing on slow time scales of seconds or minutes. Heterogeneous structures have also been reported in single component lipid membranes: Rappolt *et al.* observed gel- liquid crystal phase co-existence in a DPPC membrane by driving the system far from equilibrium by an infrared temperature jump.[20] Pabst *et al.* observed co-existence of orthorhombic and hexagonal lamellar gel phases in single component DSPG membranes.[21] The experiments point, however, to a kinetically trapped, out-of-equilibrium state, which lead to an interdigitated, stable (on the time scale of the experiments) phase. The origin of the driving force behind phase separation in artificial and biological membranes is highly debated, as "rafts", thus far, have primarily been experimentally observed in either raft forming mixtures or far from equilibrium. Phase separation in biological membranes has very recently been related to non-equilibrium fluctuations of the cytoskeleton,[22] which are coupled to the local membrane curvature. Microdomains, on the order of 10–100 nm, have been theoretically predicted and small (75 nm), transient (250 msec) domains have indeed been observed in a biological membrane *in vivo* using particle tracking techniques.[23]

The aim of this work was to experimentally prove the existence of heterogeneities in a lipid membrane, which are (1) "small" (3–50 nm), (2) transient and (3) occur in thermal equilibrium under conditions that mimic physiological conditions, such as high hydration and high temperature. Those domains would be very difficult to "see" with standard techniques, however, they are speculated to occur in biological membranes and thought to be

[a]*Department of Physics and Astronomy, McMaster University, Hamilton, ON, L8S 4M1, Canada. E-mail: armstc5@mcmaster.ca; rheinstadter@mcmaster.ca; Fax: +(905)546-1252; Tel: +(905)525-9140 ext.23134*
[b]*Canadian Neutron Beam Centre, National Research Council, Chalk River, ON, K0J 1J0, Canada*
[c]*Neutron Scattering Science Division, Oak Ridge National Laboratory, Oak Ridge, TN, 37831-6100, USA*
[d]*Institut Laue-Langevin, 6 rue Jules Horowitz, B.P. 156, 38042 Grenoble Cedex 9, France*

physiologically relevant.[1–4] It has been speculated that small transient domains in phospholipid model membranes are responsible for the so-called pseudo-critical behaviour, without experimental proof so far.

Phospholipid bilayers are known to undergo an acyl-chain melting transition, the so-called main transition, from an ordered gel to a disordered fluid phase. Critical fluctuations and critical swelling—most likely due to co-existent gel and fluid domains—have been reported close to this phase transition.[24–38] These lipid bilayers are, therefore, ideal model systems for the study of domain formation. The system can be tuned through the gel-fluid phase co-existence region, simply by changing the temperature, as sketched in Fig. 1.

In this paper we use the coherence length of the neutron beam to clearly show direct experimental evidence for the co-existence of gel and fluid nanodomains in the temperature range of the main phase transition. While a continuous transition between the gel and fluid phase, and a pseudo-critical behaviour have been previously reported in the literature,[24–38] we observe co-existing gel and fluid domains indicative of a first order phase transition.

In most natural systems partially coherent waves are common. X-rays and neutrons have coherence lengths that are usually significantly longer than molecular lattice spacings, including protein-protein distances in biological membranes. The coherence of waves in periodic systems (lattices) is critical with regard to their dynamics, as interference effects, such as Bragg reflections, largely determine their propagation. Additionally, in less well ordered systems, the coherence length of the probe, ξ, may play an important role in the investigation of small structures, *i.e.*, when ξ is comparable to the size of the object in question.

A collimated beam of neutrons obtained by Bragg reflection from a single crystal, or a pair of phased Fermi choppers, is never 100% monochromatic. With regard to their wave properties, their longitudinal coherence length, ξ, is defined by eqn (1):[39]

$$\xi = \frac{\lambda^2}{\Delta\lambda}. \quad (1)$$

The energy of a neutron (in meV) with wavelength λ (in Å) is given by $E = 81.81/\lambda^2$,[40] such that

$$\frac{\Delta E}{E} = 2\,\frac{\Delta\lambda}{\lambda}, \quad (2)$$

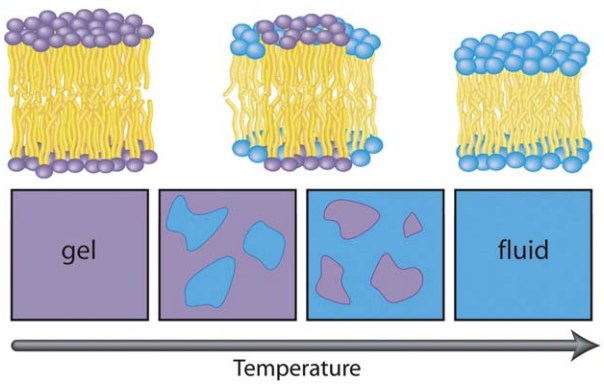

Fig. 1 Schematic of the gel-fluid transition in phospholipid membranes with co-existing gel and fluid domains.

where E is the incident neutron energy and ΔE is the instrumental energy resolution and will be discussed in more detail below. ξ can now be written as a function of E and ΔE, as follows:

$$\xi = \frac{2E}{\Delta E}\,\lambda = \frac{2E}{\Delta E}\sqrt{\frac{81.81}{E}} \sim \frac{18\sqrt{E}}{\Delta E}. \quad (3)$$

For cold neutrons with energies of ~4.5 meV and a typical monochromaticity by single crystal reflection of about 2%, the longitudinal coherence length is calculated to be approximately 450 Å (using eqn (3)). † Note, that the reason for the typically low monochromaticity of neutron beams is to avoid further compromising the already low flux "white" neutron beam, a situation that is very different for synchrotron X-rays. The longitudinal coherence length of X-rays reflected from a Si(111) monochromator with a wavelength resolution of $\Delta\lambda/\lambda \approx 1 \times 10^{-4}$ and $\lambda = 1$ Å is of the order of $\xi_{xray} = 10{,}000$ Å. The coherent properties of the scattering probe may play an important role for the investigation of small structures, such as nanoscale domains, comparable to or smaller than a given ξ – structures smaller than ξ may give spatially averaged values of, *e.g.*, peak positions and widths.

We investigated the packing and correlations of the lipid acyl chains in multi-lamellar phospholipid bilayers using neutron diffraction. DPPC, with two fully saturated acyl chains (di-16 : 0), was chosen for this study. Chain deuterated DPPC (DPPC-d62) was used to enhance out-of-plane and in-plane Bragg diffraction. By varying the coherence length of the incident neutron beam, we present direct experimental evidence for the co-existence of nanometer sized domains in single-component phospholipid membranes at temperatures close to the main phase transition. This technique can, in the future, be used to study rafts in membranes containing cholesterol and other lipid mixtures, and eventually in biological membranes.

2 Materials and methods

2.1 Sample preparation

Highly oriented multi-lamellar stacks of 1,2-dipalmitoyl-sn-*glycero*-3-phosphocholine (DPPC) were prepared on 2″ single-side polished Si wafers with a thickness of 300 μm. The coherent scattering of the lipid hydrocarbon chains was enhanced by using partially, tail deuterated lipids, *i.e.*, DPPC-d62. A solution of 20 mg mL^{-1} DPPC-d62 in 1 : 1 chloroform and 2,2,2-trifluoroethanol (TFE) was prepared. The Si wafers were cleaned by alternate 12 min sonications in ultra pure water and ethanol at 313 K. This process was repeated twice. 1 mL of the lipid solution was deposited on each Si wafer and allowed to dry. The wafers were kept in vacuum overnight to remove all traces of the solvent. The samples were then hydrated with heavy water, D_2O, and annealed in an incubator at 303 K for 24 h. Following this

† Note that the transverse coherence length ξ_t can be estimated to be $\xi_t \sim \lambda/\alpha$, where α is the divergence of the neutron beam. Long transverse coherence lengths of several micrometers are achieved in small angle neutron scattering (SANS) instruments by using small pinholes. The transverse coherence length in our setup is of the order of ~5 Å and small compared to the longitudinal coherence, as given in the Table to Fig. 2.

protocol, each wafer contained roughly 3 000 highly oriented stacked membranes with a total thickness of ~10 μm.

Twenty such Si wafers were stacked with 0.6 mm aluminium spacers placed in between each wafer to allow for the membranes to be hydrated. The "sandwich" sample was kept in a temperature and humidity controlled aluminium chamber. Hydration of the lipid membranes from the vapour phase was achieved by separately adjusting the temperature of the heavy water reservoir, the sample and the chamber cover. Temperature and humidity sensors were installed close to the sample. A water bath was used to control the temperature of the water reservoirs, and the temperature of the sample and its cover was controlled using Peltier elements. d_z-spacings of $d_z^{gel} = 70$ Å at 303 K and $d_z^{fluid} = 56$ Å at 315 K were achieved using this set-up. From values for d_z as function of relative humidity (RH) published for DMPC,[41] the hydration of the DPPC bilayers in this experiment can be estimated to better than 99.6%, close to full hydration. The main transition temperature, T_m, of deuterated DPPC is 310.5 K,[42] a value slightly lower than its protonated counterpart (T = 314.4 K).[24,42] The temperature of the pre-transition from the L_β to the $P_{\beta'}$ phase in deuterated DPPC-d62 was determined to be 302.9 K.[42] All measurements in this work were, therefore, done in the $P_{\beta'}$ and fluid L_α phase.

The samples were mounted vertically in the neutron beam such that the scattering vector (**Q**) could either be placed in the membrane plane ($\mathbf{q}_\parallel$), or perpendicular to the membrane ($\mathbf{q}_z$). Out-of-plane and in-plane structure could be measured by simply rotating the sample by 90 degrees.

2.2 Neutron experiment

Experiments were conducted using the N5 triple-axis spectrometer at the Canadian Neutron Beam Centre (Chalk River, ON, Canada). The three axis of the spectrometer refer to the axis of rotation of the monochromator, the sample and the analyzer. The incident and final neutron energies are defined by the Bragg reflections from pyrolytic graphite (PG) crystals. The divergence of the neutron beam is controlled by several neutron Soller collimators. A schematic of the instrument configuration is shown in Fig. 2. To achieve the different coherence lengths (eqn (3)) the energy of the incident neutrons and the energy resolution of the spectrometer must be varied. The incident energy is determined by the angle of reflection of the monochromator. To avoid higher order contributions, which also fulfil the Bragg condition, *i.e.*, $\lambda/2$, $\lambda/3$, a PG filter was used after the monochromator. Two incident energies were available using this setup, 14.5 meV and 42.3 meV, corresponding to neutron wavelengths of 2.37 Å and 1.39 Å respectively.

The energy resolution of a neutron triple-axis spectrometer is determined by: (1) the incident energy of the neutron beam; (2) the divergence of the neutron beam; and (3) the wavelength resolution of the monochromator and analyzer. The collimation was defined in four different regions of the beam path (c1, c2, c3, c4), as shown in Fig. 2. The tighter the collimation the better the energy resolution, however, this is achieved at the cost of a reduced neutron flux. In addition, the choice of a Bragg reflection plays a role in the energy resolution. In the case of PG

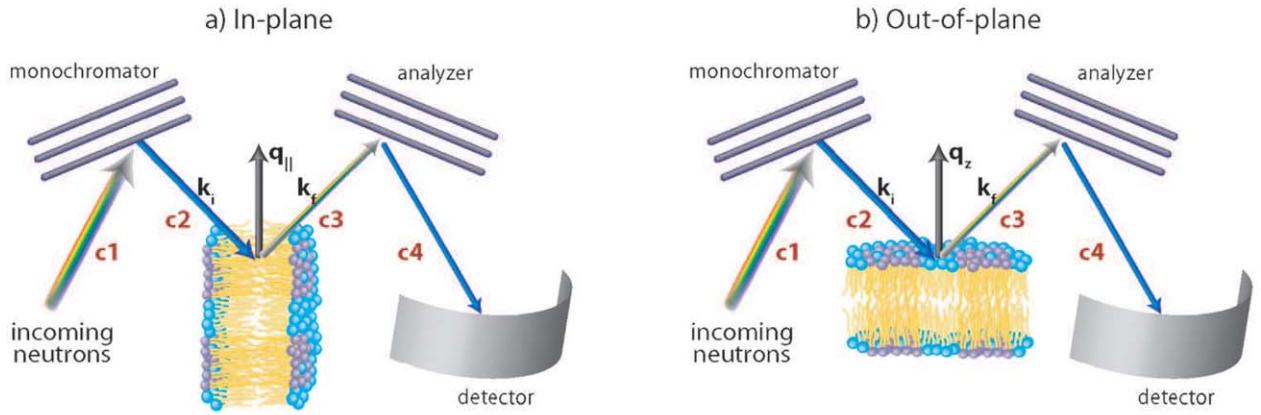

ξ (Å)	Monochromator	Analyzer	Collimation (minutes) (c1-c2-c3-c4)	Wavelength (Å)	Incident Energy (meV)	Energy Resolution ΔE (meV)	Q Resolution ΔQ (Å^{-1})
30	PG(002)	PG(002)	30-18-28-60	1.39	42.3	3.915	0.032
33	PG(004)	PG(002)	30-18-28-60	1.39	42.3	3.504	0.032
46	PG(002)	PG(004)	30-18-28-60	1.39	42.3	2.524	0.032
64	PG(004)	PG(004)	30-18-28-60	1.39	42.3	1.821	0.033
103	PG(004)	PG(002)	30-18-28-60	2.37	14.5	0.6643	0.018
152	PG(002)	PG(004)	30-18-28-60	2.37	14.5	0.451	0.019
242	PG(004)	PG(004)	30-18-28-60	2.37	14.5	0.2836	0.019

Fig. 2 Geometry of the triple axis spectrometer. a) Orientation of the sample for in-plane scans, such that **Q** is in the plane of the membrane ($\mathbf{q}_\parallel$). b) Orientation of the sample for out-of-plane scans, such that **Q** is perpendicular to the plane of the membrane ($\mathbf{q}_z$). The table displays the instrumental settings used to achieve the different coherence lengths, ξ, using eqn (3). k_i and k_f are the incident and final neutron wave vectors ($k = 2\pi/\lambda$).

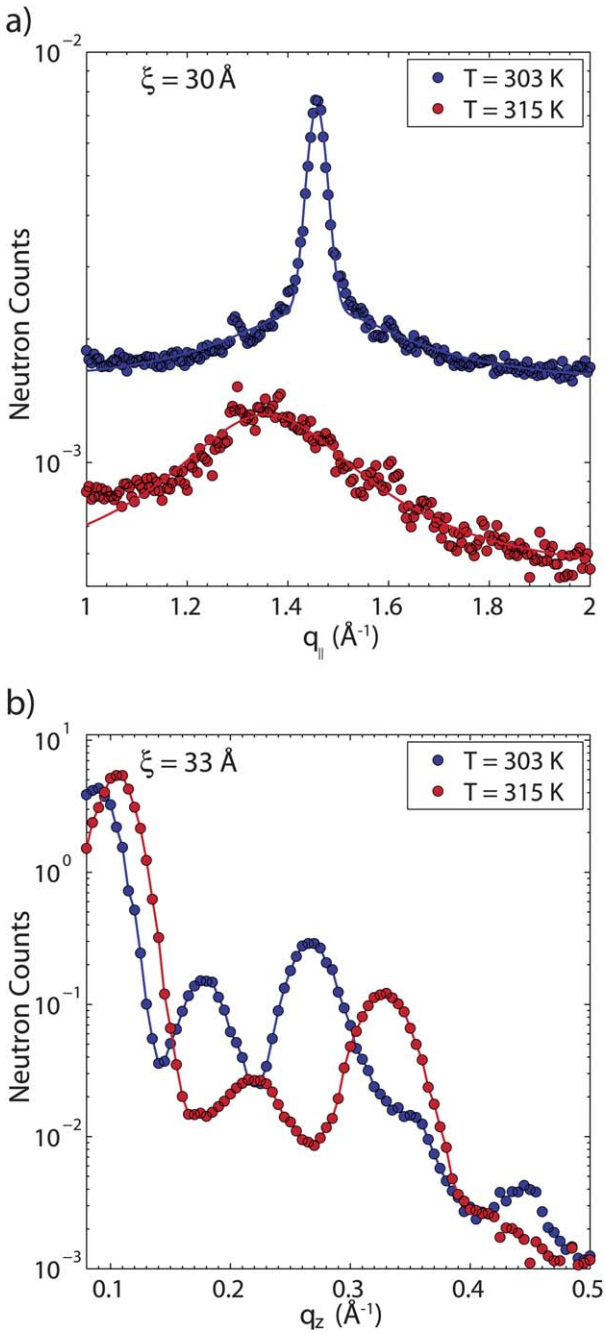

Fig. 3 Scans of gel and fluid DPPC bilayers at $T = 303$ K and $T = 315$ K, respectively. a) In-plane ($q_{||}$) scan showing the lipid acyl chain correlation peak. b) Out-of-plane (q_z) curves displaying the change in d_z-spacing between gel and fluid phase bilayers.

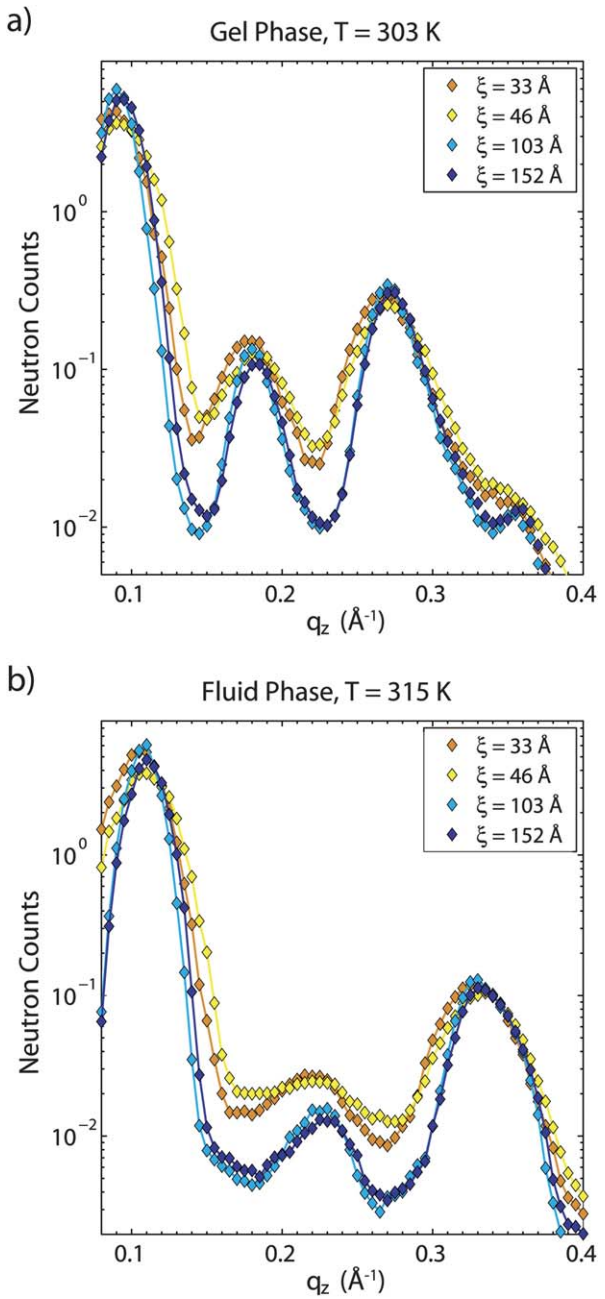

Fig. 4 Out-of-plane scattering curves of stacked DPPC-d62 membranes probed with different coherence length neutrons (33 Å< ξ < 152 Å). a) Gel phase and b) fluid phase bilayers. Curve shapes change as a function of q_z resolution, as listed in the Table to Fig. 2.

crystals, both the PG(002) and PG(004) reflections can be used for monochromatization. According to Bragg's law, the energy resolution is improved with higher angles of reflection (*i.e.* PG(004)), which also happens to reduce neutron flux. The table in Fig. 2 lists the different configurations used and their corresponding coherence lengths.

Collimation was kept constant during the course of the experiment. Coherence lengths between 30 and 242 Å were achieved by using different incident energies and two different PG reflections. The momentum resolution, ΔQ, is also given in the Table to Fig. 2. A good Q resolution usually implies the use of fine collimation and a corresponding large coherence length. In order to enable small nanometer sized structures to become visible, poor energy and Q resolution are needed, which at first sounds counter intuitive – to be discussed later.

3 Results

Fig. 3 shows the in-plane (a) and out-of-plane (b) measurements of gel phase ($T = 303$ K) and fluid phase ($T = 315$ K) DPPC

membranes. The in-plane scan depicts the lipid acyl chain correlation peak, which is the result of the close packed lipid tails making up the hydrophobic membrane core. The correlation peak occurs at 1.46 Å^{-1} in the gel phase, and at 1.37 Å^{-1} in the fluid phase, corresponding to nearest neighbour distances of 4.3 Å and 4.6 Å. The narrow width of the gel peak indicates a well-ordered structure; the peak broadens significantly and loses intensity in the fluid phase of the bilayers due to increased fluctuations.[38] The d_z-spacing between two neighbouring membranes in the stack can be determined from the spacing between the well developed Bragg reflections ($d_z = 2\pi/\Delta q_z$) in the out-of-plane curves in Fig. 3 (b). d_z-spacings of 70 Å and 56 Å are observed for gel and fluid DPPC bilayers, respectively, and the data were obtained with a neutron coherence length of 33 Å.

Fig. 4 depicts out-of-plane curves in the gel and fluid phase measured at different coherence lengths. The peaks are well described by Gaussian peak profiles. The broadening of the peaks changes slightly due to the difference in q_z resolution, as listed in the Table in Fig. 2. However, the position of the Bragg peaks in the different out-of-plane curves does not change as a function of ξ. The resolution (and coherence properties) of the neutron spectrometer are, therefore, not crucial in determining membrane structure deep in the gel or the fluid phase.

The in-plane structure of bilayers in the vicinity of the main phase transition temperature, T_m, was investigated in more detail (Fig. 5). Only one correlation peak at $q_{\|} = 1.46$ Å^{-1}, corresponding to the gel phase is observed at $T = 303$ K. When increasing the temperature, a second correlation peak appears at

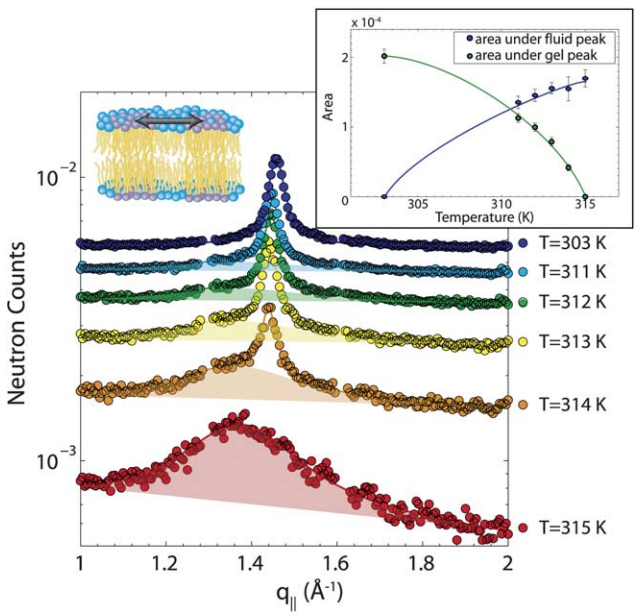

Fig. 5 In-plane scans of DPPC-d62 bilayers at 303 K<T<315 K. (Aluminium Bragg peaks from the humidity chamber were cut out at around $q_{\|} = 1.3$ and 1.6 Å^{-1} for clarity.) Correlation peaks corresponding to co-existing gel and fluid phases are observed close to the main transition temperature, T_m ($\xi = 30$ Å). The inset to the figure displays the area under the fluid and gel peaks, determined from fits of Lorentzian profiles, as a function of temperature. Note that the in-plane scans are plotted on a logarithmic scale to make the broad lipid peak more visible. The corresponding areas are displayed using a linear y-axis.

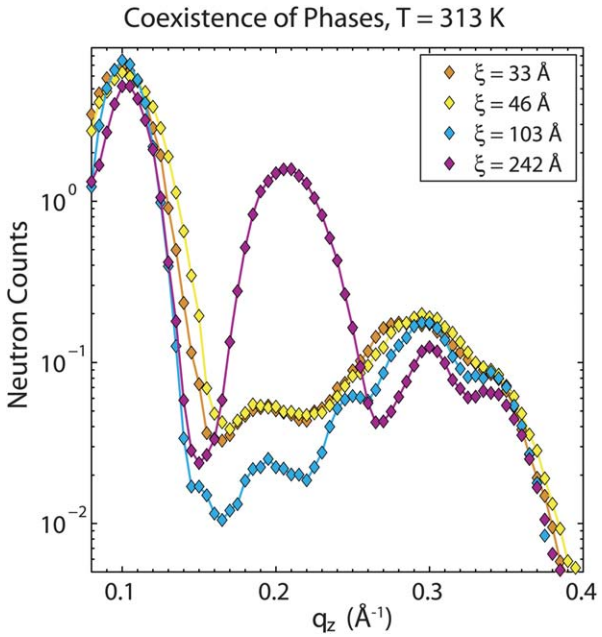

Fig. 6 Out-of-plane scattering curves resulting from stacked DPPC membranes near the main transition temperature ($T_m = 313$ K), probed with different neutron coherence lengths, ξ. The three well-developed, out-of-plane Bragg peaks observed with $\xi = 242$ Å split when the coherence length is reduced to $\xi \leq 103$ Å.

the nominal fluid position ($q_{\|} = 1.37$ Å^{-1}). The intensity of the gel peak is reduced with increasing temperature, while the fluid peak increases. Only the fluid peak is observed at $T = 315$ K. The data in Fig. 5, measured using a small coherence length, show the co-existence of the gel and the fluid peaks with increasing temperature. The area under the correlation peaks, which was determined from fits of Lorentzian peak profiles, is proportional to the volume of their respective phases, and are graphically depicted in the inset to Fig. 5. The fluid phase grows when heating through the transition at the cost of gel phase domains. Based on this data, the co-existence region extends from ~311–314 K.

Out-of-plane curves at $T = 313$ K are shown in Fig. 6. The data measured at high energy and q_z resolution, with a ξ of 242 Å, show three well-defined Bragg peaks with a d_z spacing of 63 Å. We note that this d_z-spacing is the average between d_z^{gel} and d_z^{fluid} ((70 Å + 56 Å)/2 = 63 Å) as determined from gel and fluid phase data (in Fig. 3 (b)). At smaller coherence lengths ξ, however, a peak splitting is observed. Each of the out-of-plane Bragg peaks splits into several separate reflections. The splitting occurs between 103 Å< ξ < 242 Å. Although the width of the Bragg reflections is resolution limited, the Bragg width of the ξ = 242 Å reflection is considerably broader than the instrumental resolution (given in the Table of Fig. 2). Significant peak broadening with improving q_z resolution is consistent with the averaging of individual Bragg peaks.

4 Discussion

The transition from gel ($P_{\beta'}$) to fluid (L_α) phospholipid bilayers has previously been reported to show critical behavior ("critical

swelling").[24–38] The lamellar spacing d_z, but also the nearest neighbour distance of lipid molecules in-the-plane of the membrane, mimic the critical behaviour observed in second order magnetic order-disorder transitions.[38] Critical behaviour is expected in second order phase transitions, with no co-existence of low and high temperature phases. However, a latent heat has been found in the main transition of phospholipid bilayers, which clearly identifies this transition as being of first order.[24–26] The observation of a pseudo-critical behaviour has, therefore, been puzzling and has resulted in a lively and ongoing debate in the literature.

Experimental evidence for co-existing gel and fluid domains has been reported. Inelastic neutron experiments on DMPC previously reported evidence for the co-existence of small nanometer gel and fluid domains in the temperature range of the main phase transition[38] – based on the co-existence of the corresponding excitations in the spectra. The long wavelength dispersion relation, as measured with a neutron spin-echo spectrometer, showed a pronounced soft mode at a length scale of about 420 Å.[8] It was speculated that domains may be responsible for the extreme softness, *i.e.*, the very low value for the bending modulus of phospholipid bilayers in the range of the phase transition, known as "critical softening".[34] Bending of the membrane most likely occurs at the interface between two nanodomains, which costs less energy than bending a pure gel or fluid domain. The diameter of these domains can be estimated to be 420 Å from this experiment. The relaxation rate of domain pattern fluctuations of aqueous solutions of vesicles near the fluid-gel phase transition temperature was found to show a pronounced slowing near the main phase transition in ultrasonic spectra.[10] Finally, co-existing gel and fluid domains in single-component lipid membranes were also reported from computer simulations.[12,43]

The two in-plane Bragg peaks shown in Fig. 5 present direct experimental evidence for co-existing gel and fluid domains in single-component phospholipid bilayers in the range of the main phase transition. Based on the lengths scales accessible in this experiment, limits for the domain size can be determined. The longest coherence length available in this experiment indicates that the lower limit for the size of those domains is ~242 Å in diameter, which is in good agreement with estimated values determined by the neutron spin-echo measurements.[8] However, because the smallest available neutron coherence length was 30 Å, our experiment can not rule out the existence of even smaller structures that include only a few lipid molecules. Instead of a critical behaviour with a continuously shifting peak, as was reported by Rheinstädter *et al.*,[38] we observe the co-existence of gel and fluid like domains, with their ratio changing as a function of temperature. The main transition in phospholipid membranes was, therefore, found to show the characteristics of a first order phase transition, in agreement with calorimetric experiments[24–26]

In out-of-plane scattering experiments, with good momentum resolution and corresponding high neutron coherence length, a continuous change of the lamellar d_z spacing is observed, as depicted in Fig. 6 for a coherence length of $\xi = 242$ Å, while a splitting of the Bragg peaks is observed at smaller coherence lengths. In the pure gel or fluid phase, all neighbouring membranes are in the same state, although different scenarios may develop in the transition region. The two neighbouring

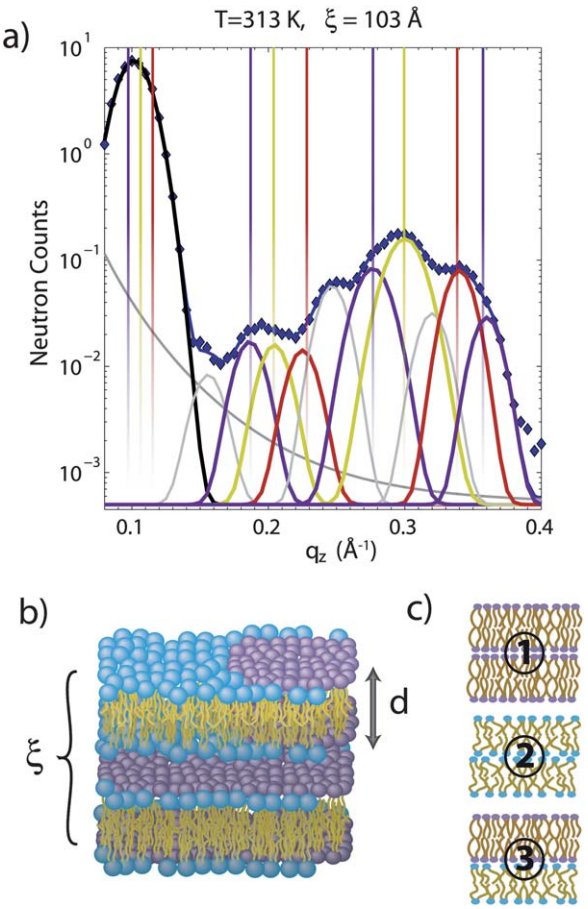

Fig. 7 a) Out-of-plane scattering curves of stacked DPPC membranes near the transition temperature ($T = 313$ K), probed with a coherence length of $\xi = 103$ Å. Fitting of the data reveals Bragg peaks from the different phases: fluid, gel, and intermediate phases. No fine structure of the first Bragg peak at around $q_{\|} = 0.10$ Å^{-1} could be resolved; it is, therefore, fit by a single peak (black line). Bragg peaks corresponding to the gel phase bilayers are shown in purple, those corresponding to fluid phase bilayers are shown in red, and those corresponding to mixed phase bilayers are shown in yellow. Additional peaks are shown in grey. b) Sketch of the multi-lamellar membrane patch with co-existing gel and fluid domains. c) Illustration of the three possible stacking scenario. Scenario 3 results in a d_z space which is the average of the fluid and gel spacing.

membranes may be: (1) both in the gel phase; (2) both in the fluid phase; or (3) one in the gel phase and the other in the fluid phase. The three scenarios are depicted in Fig. 7 c). When a gel region of the bilayer happens to be next to a fluid region, a long neutron coherence length (greater than $d_z^{gel} + d_z^{fluid}$) will average over the two d_z-spacings and result in an average d_z value between d_z^{gel} and d_z^{fluid}. The d_z spacing of 63 Å at $T = 313$ K, therefore, points to a multi-lamellar membrane structure with neighbouring gel and fluid domains. Based on this assumption, the critical coherence length ξ can be estimated to equal 126 Å. For ξ less than 126 Å, the neutron coherence only covers a single membrane, as shown in Fig. 7 b).

Fig. 7 shows a fit of the out-of-plane scattering curve measured at $\xi = 103$ Å (Fig. 6). Eleven Bragg peaks can be identified and could be fit to the data and assigned to different d_z spacings and

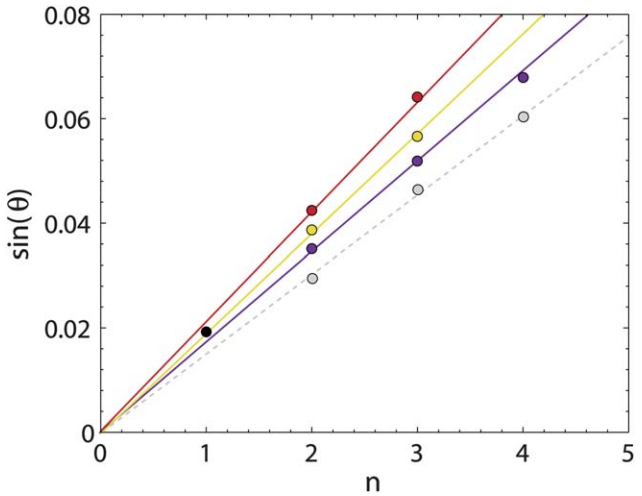

Fig. 8 Plot of $s\,i\,n\,(\theta) = \lambda n/2\,d$. Peaks belonging to the same d_z-spacing fall on a straight line through the origin. The 11 Bragg peaks fit in Fig. 7 a) can be assigned to 4 different d-spacings, namely, 56 Å, 63 Å, 70 Å, and 77 Å.

phases. To assign the peaks to different phases, Bragg's law can be re-written as $s\,i\,n\,(\theta) = \lambda n/2\,d$. Therefore, by plotting $sin(\theta)$ *vs.* the (estimated) order of the different Bragg reflections (n), peaks which belong to the same d_z-spacing will fall on a straight line through the origin. This plot is shown in Fig. 8. The 11 Bragg peaks can be assigned to 4 different d_z-spacings, namely, 56 Å, 63 Å, 70 Å, and 77 Å. The d_z spacings of 70 Å and 56 Å agree perfectly with the d_z spacings found in gel and fluid phase. The intermediate phase, with a d_z spacing of 63 Å, can be assigned to scenario (3), with neighbouring gel and fluid domains in the membrane stack. There is an additional series of reflections in Fig. 8. These peaks fall on a line through the origin with a slope corresponding to a d_z spacing of 77 Å. This d_z spacing does not correspond to one of the three proposed scenarios, gel, fluid and gel–fluid. However, it is well known that unexpected or quasi-forbidden Bragg peaks can appear in soft materials[44] to adapt to macroscopic constraints. The melting of a membrane patch from the gel to the fluid state inside a stack of membranes is sketched in Fig. 7 b). The size difference between d_z^{gel} and d_z^{fluid} would create a distortion of the multi-lamellar structure. Because the membrane stack is an elastic medium, this is associated with an energy cost. One way for the system to comply with the macroscopic constraints is to try to keep the overall thickness constant, by creating membranes with a larger d_z spacing to compensate for the difference $d_z^{gel} - d_z^{fluid}$. The observed spacing of $d_z = 77$ Å may correspond to the thickness of a DPPC bilayer where all the lipids are in all-*trans* configuration (*i.e.*, fully stretched out). This type of structure is not energetically favourable at high temperatures and just a consequence of the macroscopic constraints given by the membrane stack.

A comment is in order. Following the Gibbs' Phase Rule in condensed systems (without a co-existing gas phase) the number of independent intensive properties (F), such as temperature and pressure, depends on the number of components (C), and the number of co-existing phases in thermal equilibrium (P): F = C − P + 1. The observation of co-existing domains over a given temperature interval in a single lipid system implies F = 0, *i.e.*, a single point in temperature-pressure phase space (critical point). This observation of co-existing gel and fluid domains over a certain temperature range, therefore, seems to contradict the phase rule. Gibbs' rule, however, does not apply to *transient*, short lived domains, as discussed by Ehrig *et al.*[11] The fluctuation period of these transient domains was determined to be ∼10 ns from experiment[10] (DMPC bilayers) and MD simulations[12] (DPPC bilayers). By tuning the energy resolution ΔE in the Table in Fig. 2, the neutron diffraction experiments can also become temporally sensitive. Time resolution is defined by $\tau = \hbar/\Delta E$. As the energy resolution is ∼1 meV, only structures which fluctuate at times slower than 1 picosecond will lead to correlation peaks. The lower limit for the lifetime of the fluctuating structures observed in our experiment is, therefore, determined to be ∼1 picosecond, in agreement to the MD simulations.

While this experiment proves the co-existence of domains in single-component phospholipid bilayers, future experiments will be conducted in multi-component lipid membranes and membranes containing cholesterol to detect possible raft structures. By scanning the neutron coherence length ξ, the size of those structures will be determined using the technique developed in this work.

5 Conclusions

The coherent properties of photons and neutrons are used to study structure and dynamics in elastic and inelastic X-ray and neutron scattering experiments. Matching the coherent properties of the scattering probe with those of the sample becomes important in soft-matter and biology because of: (1) the missing long ranged order; and (2) the large length scales involved. Good monochromaticity is a prerequisite for atomic resolution in crystal and protein structure determinations. Such radiation is also highly coherent with large coherence lengths, of the order of several thousands of Angstroems. A large coherence length may, however, average over small structures, such as nanoscale domains. By controlling ξ in a neutron diffraction experiment, we present direct experimental evidence for co-existing gel and fluid domains in a phospholipid bilayer. Instead of a continuous phase transition from the well ordered gel into the fluid phase, which adheres to a well-known critical behaviour, we observe a first order transition with a co-existence of gel and fluid domains.

Nanodomains are not only important to understand fundamental properties of model membranes, but also to better understand complex biological membranes and the formation and function of lipid rafts.[4,45,46] Additional examples are the recently emerging nanoferroelectrics[47] and nanoscale magnetic domains in thin magnetic films.[48] The development of neutron instrumentation which enables the control of the neutron coherence length can be envisioned for the future. Such an instrument would not only be important for the investigation of biological materials, but in all systems where fluctuating nanodomains determine material properties.

Acknowledgements

We thank the Canadian Neutron Beam Centre for the allocation of beam time and the staff at CNBC for their support. This

research was partially funded by the Natural Sciences and Engineering Research Council of Canada (NSERC), the Canada Foundation for Innovation (CFI), the Ontario Ministry of Economic Development and Innovation, and the National Research Council Canada (NRC). John Katsaras is supported through ORNL's Laboratory Directed Research and Development (LDRD), and Program Development programs.

References

1 D. M. Engelman, *Nature*, 2005, **438**, 578–580.
2 D. Lingwood and K. Simons, *Science*, 2009, **327**, 46–50.
3 K. Simons and E. Ikonen, *Nature*, 1997, **387**, 569–572.
4 C. Eggeling, C. Ringemann, R. Medda, G. Schwarzmann, K. Sandhoff, S. Polyakova, V. N. Belov, B. Hein, C. von Middendorf, A. Schönle and S. W. Hell, *Nature*, 2009, **457**, 1159–1162.
5 P.-F. Lenne and A. Nicolas, *Soft Matter*, 2009, **5**, 2841–2848.
6 T. Apajalahti, P. Niemelä, P. N. Govindan, M. S. Miettinen, E. Salonen, S.-J. Marrink and I. Vattulainen, *Faraday Discuss.*, 2010, **144**, 411–430.
7 E. Watkins, C. Millerb, J. Majewski and T. Kuhl, *Proc. Natl. Acad. Sci. U. S. A.*, 2011, **108**, 6975–6980.
8 M. C. Rheinstädter, W. Häussler and T. Salditt, *Phys. Rev. Lett.*, 2006, **97**, 048103.
9 P. S. Niemel, S. Ollila, M. T. Hyvnen, M. Karttunen and I. Vattulainen, *PLoS Comput. Biol.*, 2007, **3**, e34.
10 B. Bruning, E. Wald, W. Schrader, R. Behrends and U. Kaatze, *Soft Matter*, 2009, **5**, 3340–3346.
11 J. Ehrig, E. P. Petrov and P. Schwille, *New J. Phys.*, 2011, **13**, 045019.
12 T. Murtola, T. Róg, E. Falck, M. Karttunen and I. Vattulainen, *Phys. Rev. Lett.*, 2006, **97**, 238102.
13 G. Pabst, N. Kučerka, M.-P. Nieh, M. C. Rheinstädter and J. Katsaras, *Chem. Phys. Lipids*, 2010, **163**, 460–679.
14 G. Fragneto and M. Rheinstädter, *C. R. Phys.*, 2007, **8**, 865–883.
15 J. Pencer, T. Mills, V. Anghel, S. Kruegar, R. Epand and J. Katsaras, *Eur. Phys. J. E*, 2005, **18**, 447–458.
16 J. Pencer, V. Anghel, N. Kucerka and J. Katsaras, *J. Appl. Crystallogr.*, 2006, **39**, 791–796.
17 V. Anghel, N. Kucerka, J. Pencer and J. Katsaras, *J. Appl. Crystallogr.*, 2007, **40**, 513–525.
18 J. Pencer, V. Anghel, N. Kucerka and J. Katsaras, *J. Appl. Crystallogr.*, 2006, **39**, 791–796.
19 C. Nicolini, P. Thyagarajan and R. Winter, *Phys. Chem. Chem. Phys.*, 2004, **6**, 5531–5534.
20 M. Rappolt, G. Pabst, G. Rapp, M. Kriechbaum, H. Amenitsch, C. Krenn, S. Bernstroff and P. Laggner, *Eur. Biophys. J.*, 2000, **29**, 125–133.
21 G. Pabst, S. Danner, G. Deutsch and A. Raghunathan, *Biophys. J.*, 2007, **93**, 513–525.
22 P. Sens and M. Turner, *Phys. Rev. Lett.*, 2011, **106**, 238101.
23 A. Sergé, N. Bertaux, H. Rigneault and D. Maruet, *Nat. Methods*, 2008, **5**, 687–694.
24 S. Mabrey and J. Sturtevant, *Proc. Natl. Acad. Sci. U. S. A.*, 1976, **73**, 3862–3866.
25 S. Andersen, A. Jackson and T. Heimburg, *Prog. Neurobiol.*, 2009, **88**, 104–113.
26 T. Heimburg and D. Jackson, *Proc. Natl. Acad. Sci. U. S. A.*, 2005, **102**, 28.
27 P. Mason, J. Nagle, R. Epand and J. Katsaras, *Phys. Rev. E: Stat. Phys., Plasmas, Fluids, Relat. Interdiscip. Top.*, 2001, **63**, 030902.
28 G. Pabst, J. Katsaras, V. A. Raghunathan and M. Rappolt, *Langmuir*, 2003, **19**, 1716–1722.
29 R. Zhang, W. Sun, S. Tristram-Nagle, R. L. Headrick, R. M. Suter and J. F. Nagle, *Phys. Rev. Lett.*, 1995, **74**, 2832–2835.
30 J. Lemmich, K. Mortensen, J. Ipsen, T. Hø nger, R. Bauer and O. Mouritsen, *Phys. Rev. Lett.*, 1995, **75**, 3958.
31 F. Chen, W. Hung and H. Huang, *Phys. Rev. Lett.*, 1997, **79**, 4026–4029.
32 J. Nagle, H. Petrache, N. Gouliaev, S. Tristram-Nagle, Y. Liu, R. Suter and K. Gawrisch, *Phys. Rev. E: Stat. Phys., Plasmas, Fluids, Relat. Interdiscip. Top.*, 1998, **58**, 7769–7776.
33 G. Fragneto, T. Charitat, E. Bellet-Amalric, R. Cubitt and F. Graner, *Langmuir*, 2003, **19**, 7695–7702.
34 N. Chu, N. Kučerka, Y. Liu, S. Tristram-Nagle and J. F. Nagle, *Phys. Rev. E: Stat., Nonlinear, Soft Matter Phys.*, 2005, **71**, 041904.
35 T. Salditt, *J. Phys.: Condens. Matter*, 2005, **17**, R287–R314.
36 T. Salditt, *Curr. Opin. Colloid Interface Sci.*, 2000, **5**, 19–26.
37 M. Vogel, C. Münster, W. Fenzl and T. Salditt, *Phys. Rev. Lett.*, 2000, **84**, 390–393.
38 M. Rheinstädter, C. Ollinger, G. Fragneto, F. Demmel and T. Salditt, *Phys. Rev. Lett.*, 2004, **93**, 108107.
39 H. Rauch, *Found. Phys.*, 1993, **23**, 7–36.
40 G. Squires, *Introduction to the theory of thermal neutron scattering*, Dover Publications, Inc., Mineola, New York, 1978.
41 N. Kučerka, Y. Liu, N. Chu, H. I. Petrache, S. Tristram-Nagle and J. F. Nagle, *Biophys. J.*, 2005, **88**, 2626–2637.
42 J. Katsaras, R. F. Epand and R. M. Epand, *Phys. Rev. E: Stat. Phys., Plasmas, Fluids, Relat. Interdiscip. Top.*, 1997, **55**, 3751–3753.
43 S. Leekumjorn and A. Sum, *Biochim. Biophys. Acta, Biomembr.*, 2007, **1768**, 354–365.
44 S. Förster, A. Timmann, C. Schellbach, A. Frömsdorf, A. Kornowski, H. Weller, S. Roth and P. Lindner, *Nat. Mater.*, 2007, **6**, 888–893.
45 J. Oelke, A. Pasc, A. Wixforth, O. Konovalov and M. Tanaka, *Appl. Phys. Lett.*, 2008, **93**, 213901.
46 H. J. Risselada and S. J. Marrink, *Proc. Natl. Acad. Sci. U. S. A.*, 2008, **105**, 17367–17372.
47 J. Scott, *Science*, 2007, **315**, 954–959.
48 O. Shpyrko, E. Isaacs, J. Logan, Y. Feng, G. Aeppli, R. Jaramillo, H. Kim, T. Rosenbaum, P. Zschack, M. Sprung, S. Narayanan and A. Sandy, *Nature*, 2007, **447**, 68–71.

